Dalton Transactions

ROYAL SOCIETY OF CHEMISTRY

PAPER

View Article Online
View Journal | View Issue

Cite this: *Dalton Trans.*, 2025, **54**, 14111

Merging cyclopentadienone tuning and CO to isonitrile substitution to develop photo-activated iron cyclopentadienone catalysts

Clémence Gounon, [a] Gaëtan Quintil,[a,b] Jacques Pécaut,[c] Martin Clémancey,[b] Ragnar Bjornsson, [b] Adrien Quintard*[a] and Amélie Kochem *[b]

This study explores the development and reactivity of novel iron cyclopentadienone complexes incorporating isonitrile ligands for photo-activated borrowing hydrogen (BH) catalysis. By merging strategies of cyclopentadienone tuning with isonitrile functionalization, this work aims to enhance the efficiency of photoactivation processes. New complexes featuring 4-nitrophenyl isonitrile ligands combined with electron-rich cyclopentadienones (L^2 and L^3) were synthesized and characterized through X-ray crystallography, IR, and Mössbauer spectroscopy. Despite promising structural and electronic properties, these complexes showed reduced catalytic activity compared to classical Knölker-type analogues under photoactivation, particularly in allylic alcohol functionalization and BH amine alkylation. Mechanistic studies revealed that the diminished reactivity stemmed from light-induced demetallation of the L^2 and L^3-based complexes, contrasting with the stability of their L^1-based counterparts. Adding exogenous ligands like PPh_3 mitigated this demetallation, explaining the catalytic activity of L^2 and L^3 based complexes. The findings highlight the interplay of ligand design, light activation, and catalytic performance, providing a basis for advancing sustainable photocatalysis.

Received 19th May 2025,
Accepted 8th August 2025

DOI: 10.1039/d5dt01184a

rsc.li/dalton

Introduction

In the quest for the development of eco-friendly hydrogen transfer and borrowing hydrogen synthetic processes using catalysts based on abundant metals, iron(cyclopentadienone) complexes have recently received much attention due to several key features, including their cheap and easy synthesis, handling and reactivity.[1] This reactivity can compete with noble-metal catalysts thanks to the use of redox-active cyclopentadienone ligands switching between non-aromatic and aromatic forms, allowing the iron to engage in a bi-electronic Fe(0)/Fe(II) switch that operates in hydrogen transfer reactions.[2] This crucial cooperation between the metal and the ligand allows the catalyst to abstract H_2 from a donor and to transfer it to a polar double bond such as carbonyl or imine. Over time, the versatility of these catalysts in terms of reactivity has continually increased, with applications in reactions such as reductions of carbonyls and imines, oxidations of alcohols, and borrowing hydrogen reactions, as examples.[3] Improving the catalyst efficiency *via* complex structure tuning mainly focused on cyclopentadienone ring modifications,[4] with limited studies systematically investigating the underlying effects of these modifications.[5] This is primarily due to structural alterations of the cyclopentadienone core, which often impact both its steric and electronic properties, creating challenges in developing structure–activity relationships. Recently, Funk and co-workers studied a series of (3,4-diphenylcyclopentadienone)iron carbonyl compounds with electron-donating and electron-withdrawing substituents in *para* positions of the two appended aromatic rings with minimal changes to their overall size.[6] Thanks to the exploration of their reactivity under chemical activation and elegant mechanistic studies, including kinetic isotope effect experiments and modifications to substrate electronics, they demonstrated that catalysts with electron-rich cyclopentadienone ligands reacted more quickly than those without, in both transfer hydrogenations and dehydrogenations. They could notably isolate a trimethylamine-ligated (cyclopentadienone)iron dicarbonyl compound proposed as a resting state for both hydrogenation and dehydrogenation as suggested by previous studies.[7] In comparison, fewer studies have been conducted on the modification of the iron-tricarbonyl part of the catalyst. This can be explained in part due to the fact that strong field CO ligands are required for the catalytic activity as they increase the d-orbital splitting and stabilize a low-spin iron configuration. Our group recently tackled

[a]*Univ. Grenoble Alpes, CNRS, DCM, 38000 Grenoble, France. E-mail: adrien.quintard@univ-grenoble-alpes.fr, amelie.kochem@cea.fr*
[b]*Université Grenoble Alpes, CNRS, CEA, LCBM (UMR 5249), F-38000 Grenoble, France*
[c]*Univ. Grenoble Alpes, CEA, CNRS, IRIG, SYMMES, F-38000 Grenoble, UMR 5819, France*

this problem by replacing CO ligands with electronically similar but tunable isonitrile ligands. We developed a family of various isonitrile-substituted iron cyclopentadienone complexes and investigated their reactivity.[8,9] We have notably established the successful application of monosubstituted complexes in classical borrowing hydrogen amine alkylation with alcohols and most importantly, in the development of a photo-activated multicatalytic enantioselective allylic alcohol functionalization.[10] We showed that the photoirradiation of the precatalysts leads to CO dissociation and the generation of a new active species, [FeL^1(CO)(CN-R)], and that the efficiency of the photoactivation process could be directly improved through isocyanide tuning (Fig. 1).

From these results, we hypothesized that catalyst efficiency could be enhanced by merging both strategies, *e.g.* cyclopentadienone and isocyanide tuning. In this work, we report the development and structural analysis of new complexes that incorporate the substituted isocyanide CN-Ph-NO$_2$, which has shown the most effective photo-activation process to date. These catalysts also feature either of the electron-rich L^2 and L^3 ligands, identified by Funk, Renaud and collaborators as having the best catalytic activity for hydrogenation (for L^2 and L^3 ligands)[11] and dehydrogenation (for the L^2 ligand).[6]

Results and discussion

Catalyst preparation and structural analysis

The complexes **[FeL^1(CO)$_3$]**,[12,13] **[FeL^2(CO)$_3$]**,[14] **[FeL$_3$(CO)$_3$]**[11] and **[FeL^1(CO)$_2$(CN-Ph-NO$_2$)]**[8] were prepared according to published procedures. The new complexes, **[FeL^2(CO)$_2$(CN-Ph-NO$_2$)]** and **[FeL^3(CO)$_2$(CN-Ph-NO$_2$)]**, were obtained in high yields (62 and 46%, respectively) by reacting the corresponding tris-carbonyl complexes in the presence of a slight excess of isocyanide and Me$_3$NO at room temperature in pentane. The complexes were air stable solids stored under darkness at room temperature. No decomposition was observed after several months of storage under these conditions (Scheme 1).

Single crystals of **[FeL^2(CO)$_2$(CN-Ph-NO$_2$)]** were grown by the slow diffusion of pentane into a concentrated solution of the complex in dichloromethane. Its structure and selected bond distances are shown in Fig. 2. The X-ray crystal structures of the parent complex **[FeL^2(CO)$_3$]**[14] and derivatives in which one CO has been substituted either by one trimethylamine[6] or one NHC carbene[14] ligand were previously described. In all these structures, the four aromatic rings are tilted out of the plane of the cyclopentadienone. Moreover, the replacement of one CO by a strong donor and weaker π-acceptor, such as trimethylamine or NHC ligand, induced a contraction of the remaining two Fe–CO bond distances (from an average of 1.81 Å in tris-carbonyl complex to 1.78 Å in trimethylamine monosubstituted complex to 1.76 Å in the NHC monosubstituted complex). Such contraction was also observed in **[FeL^1(CO)$_2$(CN-Ar)]** complexes where one CO ligand was replaced by an isonitrile ligand, with the extent of contraction influenced by the type of isonitrile functionalization.[8] For example, electron-poor isonitriles such as CN-Ph-NO$_2$ promoted greater π-backbonding, resulting in reduced contraction of the remaining Fe–CO bond. In **[FeL^2(CO)$_2$(CN-Ph-NO$_2$)]**, the average of the two Fe–CO bond distances is 1.79 Å, similar to its parent tris-carbonyl complex. It shows the propensity of the CN-Ph-NO$_2$ ligand to mimic the CO properties as a good σ donor and π acceptor ligand.

Next, the various complexes were studied by IR, an excellent technique to evaluate the impact of the bonding environment *via* CO and CN stretching frequency investigation. Consistent

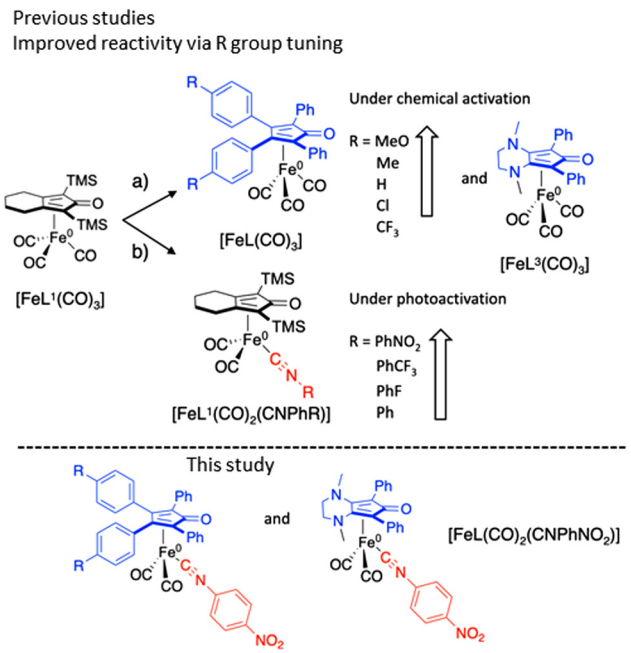

Fig. 1 Iron cyclopentadienone tuning for improved reactivity under chemical and photochemical activation (top). New iron complexes merging both strategies (bottom).

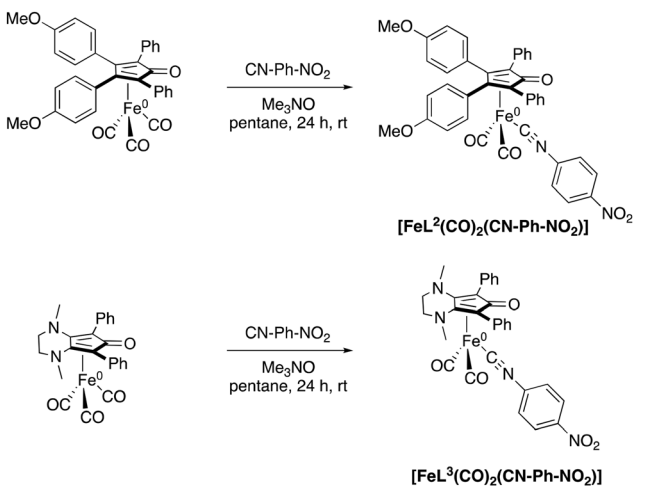

Scheme 1 Synthetic protocol to access **[FeL^2(CO)$_2$(CN-Ph-NO$_2$)]** and **[FeL^3(CO)$_2$(CN-Ph-NO$_2$)]**.

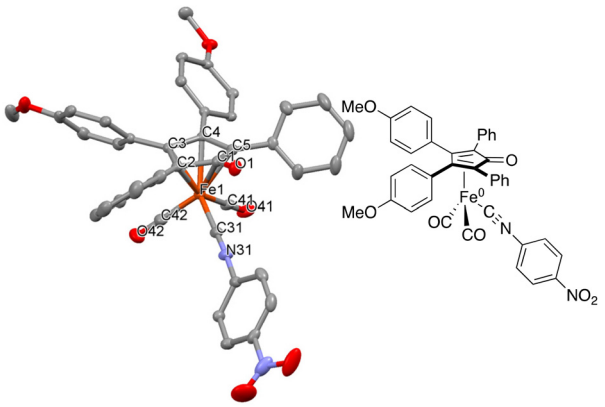

Fig. 2 ORTEP drawing of **[FeL^2(CO)$_2$(CN-Ph-NO$_2$)]**. Displacement ellipsoids are at the 30% probability level. H-atoms have been omitted for clarity. Selected bond lengths (Å): Fe(1)–C(1) 2.395(2), Fe(1)–C(2) 2.139(2), Fe(1)–C(3) 2.085(2), Fe(1)–C(4) 2.092(2), Fe(1)–C(5) 2.103(2), Fe(1)–C(31) 1.843(2), Fe(1)–C(41) 1.788(2), Fe(1)–C(42) 1.791(3), C(1)–O(1) 1.227(3), C(31)–N(31), 1.158(3), C(42)–O(42) 1.134(4), and C41–O(41) 1.134(3). Deposited at the Cambridge Crystallographic Data Centre under the number: CCDC 2419951.

with the mono-substitution of one CO by the isocyanide, the IR spectrum of **[FeL^2(CO)$_2$(CN-Ph-NO$_2$)]** exhibits one vibration band at 2130 cm^{-1} attributed to the CN stretching frequency, two absorption bands attributed to the symmetric (1997 cm^{-1}) and antisymmetric (1958 cm^{-1}) stretching frequencies of the terminal CO ligands (Fig. S1). As compared to **[FeL^1(CO)$_2$(CN-Ph-NO$_2$)]**, the νCO and νCN of the terminal ligands vibrate at similar wavenumbers in **[FeL^2(CO)$_2$(CN-Ph-NO$_2$)]** (Fig. S1 and Table 1). In **[FeL^3(CO)$_2$(CN-Ph-NO$_2$)]**, the νCO (1979 and 1929 cm^{-1}) and νCN (2089 cm^{-1}) of the terminal ligands vibrate at much lower wavelengths (Fig. S1 and Table 1). It suggests that replacing the cyclopentadienone L^1 by L^2 does not change significantly the terminal Fe–CO and Fe-isocyanide bonding which are reinforced in complexes based on the L^3 type ligand. The reinforcement of the Fe–CO bonding had been observed earlier in the parent complex **[FeL^3(CO)$_3$]** as compared to **[FeL^1(CO)$_3$]** and **[FeL^2(CO)$_3$]** and is probably due to the higher electron-enrichment of the L^3 ligand (Fig. S1).

Finally, the effect of the cyclopentadienone tuning on the electronic properties of the iron center in the series of tris-carbonyl and monosubstituted complexes was investigated by Mössbauer spectroscopy. Their spectra recorded at 80 K, complemented by that of the L$_1$ based complexes **[FeL^1(CO)$_3$]**[7] and **[FeL^1(CO)$_2$(CN-Ph-NO$_2$)]**,[8] are displayed in Fig. S2 and S3. All the complexes are characterized by a single doublet whose nuclear parameters are listed in Table 2. They all exhibit similar isomer shifts and quadrupolar splittings, except for complexes based on the L^3 type ligand, which exhibit a slightly higher isomer shift. These results show that the cyclopentadienone tuning has limited electronic impact on the iron center.

Table 1 Experimental IR frequencies for complexes **[FeL^1(CO)$_2$(CN-Ph-NO$_2$)]**, **[FeL^2(CO)$_2$(CN-Ph-NO$_2$)]** and **[FeL^3(CO)$_2$(CN-Ph-NO$_2$)]**

	$\tilde{\nu}$ [cm^{-1}]		
Iron complexes	CN	CO (*sym.*)	CO (*asym.*)
[FeL^1(CO)$_2$(CN-Ph-NO$_2$)]	2117	2007	1964
[FeL^2(CO)$_2$(CN-Ph-NO$_2$)]	2130	1997	1958
[FeL^3(CO)$_2$(CN-Ph-NO$_2$)]	2089	1979	1929

Catalyst activity

The first trials with the newly designed catalysts in borrowing hydrogen reactions, particularly in the traditional amine alkylation using alcohols, validated their catalytic activity under chemical activation (Table 3). Using 5 mol% of the iron complexes, conversion to the alkylated amine occurred with a yield of 32–47% using the mono-substituted isonitrile complexes (entries 2, 4 and 5), while all the tris carbonyl complexes provided a quantitative yield under the same conditions (entries 1, 3 and 6). The lower catalytic activity of the isocyanide-substituted complexes is not surprising and can be correlated to their more challenging chemical activation compared to their tris-carbonyl counterparts.[8]

Next, we screened the new isonitrile-substituted complexes in the condensation of dibenzoylmethane to allyl alcohol using an organocatalyst (**Org**) under 368 nm LED photoactivation as shown in Table 4. Their catalytic efficiency was compared to the complexes **[FeL^1(CO)$_3$]** and **[FeL^1(CO)$_2$(CN-Ph-NO$_2$)]** previously investigated.[8] Not surprisingly, the tris-carbonyl complexes exhibit poor, if not negligible, catalytic activity, with conversions of 0% and 13% for **[FeL^2(CO)$_3$]** and **[FeL^3(CO)$_3$]**, respectively. This is consistent with previous observations for **[FeL^1(CO)$_3$]**.[3b,8] Indeed, while this catalyst demonstrated good efficiency under chemical activation, its performance decreased under UV activation, highlighting the importance of selecting the appropriate catalyst based on the type of activation used. However, the catalytic activity of the corresponding monosubstituted complexes is more unexpected. While the introduction of the isocyanide CN-Ph-NO$_2$ in **[FeL^1(CO)$_2$(CN-Ph-NO$_2$)]** drastically increased catalytic activity under photoactivation, achieving a conversion yield of 95%, the efficiency of the new complexes **[FeL^2(CO)$_2$(CN-Ph-NO$_2$)]** and **[FeL^3(CO)$_2$(CN-Ph-NO$_2$)]** remains low, with conversion

Table 2 Mössbauer parameters determined from simulations of the spectra of tris-carbonyl and mono-substituted complexes. Only the absolute value of the quadrupole splitting can be experimentally determined from zero-field Mössbauer spectra. Uncertainties are ±0.02 mm s^{-1}, ±0.05 mm s^{-1} and ±0.02 mm s^{-1}, on δ, ΔE_Q and Γ_{fwhm}, respectively

Iron complex	δ (mm s^{-1})	ΔE_Q (mm s^{-1})	Γ (mm s^{-1})
[FeL^1(CO)$_3$]	0.06	1.46	0.29
[FeL^1(CO)$_2$(CN-Ph-NO$_2$)]	0.05	1.61	0.30/0.31
[FeL^2(CO)$_3$]	0.07	1.56	0.30
[FeL^2(CO)$_2$(CN-Ph-NO$_2$)]	0.07	1.61	0.31
[FeL^3(CO)$_3$]	0.11	1.57	0.36
[FeL^3(CO)$_2$(CN-Ph-NO$_2$)]	0.09	1.62	0.40

Table 3 Activity of selected iron complexes in amine alkylation under chemical activation

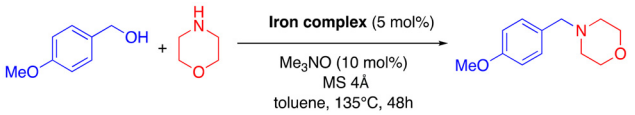

Entry	Iron complex	^{1}H NMR yield[a]	Isolated yield
1	$[FeL^1(CO)_3]$	99%	nd
2	$[FeL^1(CO)_2(CN\text{-}Ph\text{-}NO_2)]$	39%	nd
3	$[FeL^2(CO)_3]$	99%	70
4	$[FeL^2(CO)_2(CN\text{-}Ph\text{-}NO_2)]$	47%	29
5	$[FeL^3(CO)_3]$	99%	77
6	$[FeL^3(CO)_2(CN\text{-}Ph\text{-}NO_2)]$	32%	nd

[a] Determined by ^{1}H NMR using dibromomethane as the internal standard.

Table 4 Activity of iron complexes in the photo-induced functionalization of allyl alcohol

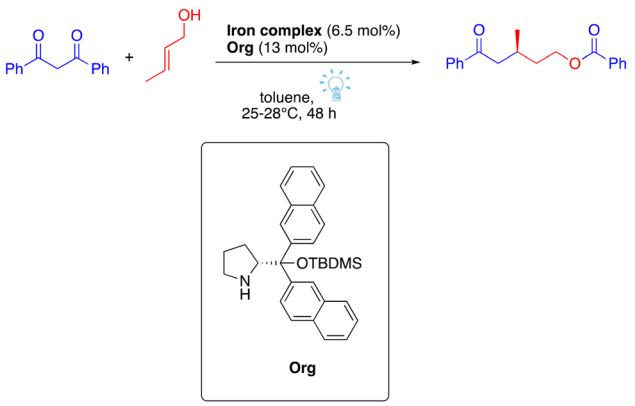

Entry	Iron complex	Conversion[a]
1	$[FeL^1(CO)_3]$	9%
2	$[FeL^1(CO)_2(CN\text{-}Ph\text{-}NO_2)]$	95%[b]
3	$[FeL^2(CO)_3]$	0%
4	$[FeL^2(CO)_2(CN\text{-}Ph\text{-}NO_2)]$	26%
5	$[FeL^3(CO)_3]$	13%
6	$[FeL^3(CO)_2(CN\text{-}Ph\text{-}NO_2)]$	12%
7[c]	$[FeL^3(CO)_2(CN\text{-}Ph\text{-}NO_2)]$	12%

Reactions performed using 0.2 mmol of diketone and 0.4 mmol of allyl alcohol in 0.325 mL of toluene over 43 hours. [a] Determined by ^{1}H NMR. [b] 88 : 12 er determined by SFC. [c] Reaction performed for 86 hours.

yields of 26% and 12%, respectively (Table 2, entry 3 and 6). Extending the reaction time did not improve the catalytic efficiency (Table 4, entry 8), indicating a potential degradation of the active catalyst over time.

The introduction of electron-rich ligands such as L^2 and L^3 has proved beneficial for the catalytic activity of the corresponding tris-carbonyl complexes under chemical activation. However, these results demonstrate that these ligands are detrimental to the reactivity of photoactivated complexes. At this stage, many fundamental questions arise concerning the structure–activity relationship. What explains this difference in reactivity? Are the activation kinetics of the precatalysts different depending on their structure or the type of activation used? Is the nature and quantity of active species formed different depending on the catalyst or the type of activation used? And can it be directly correlated to catalyst efficiency? To attempt to answer these questions, we first studied the behavior of the catalysts under light-irradiation.

Behavior and species formed under light-irradiation of the precatalyst in the absence of exogenous ligands

Initially, the absorption properties of the complexes and ligands were investigated (Fig. 3 and Table 5). The free L^1 ligand (brown line, Fig. 3) is characterized by a low absorption band at 417 nm (738 M^{-1} cm^{-1}). The free L^2 ligand (blue line, Fig. 3) is characterized by an intense absorption band at 375 nm (11 240 M^{-1} cm^{-1}) and a band of lowest intensity at 516 nm (941 M^{-1} cm^{-1}) while the diaryl L^3 ligand is characterized by an intense absorption band at 314 nm (23 395 M^{-1} cm^{-1}) and a low absorption at 509 nm (520 M^{-1} cm^{-1}).

The absorption properties of tetraarylcyclopentadienones were previously investigated.[15] All of them exhibited at least three electronic transitions with an absorption maximum changed upon substitution of the *para* positions of the phenyl rings. Thanks to computational chemistry, Hughes *et al.* attributed each of these transitions to ligand-to-ligand charge transfer excitation involving the π molecular orbitals (MOs) of the cyclopentadienone core (π to π* transitions). They notably showed that the introduction of electron-donating substituents on the *para* position of the phenyl rings induced a lowering of the transition energies λ^1 and λ^2 due to a destabilization of the π donor orbitals located at the cyclopentadienone with a π* acceptor orbital which does not vary in energy. Inspired by these works, we performed time-dependent DFT (TD-DFT) calculations. Difference density plots for the computed transitions of L^1, L^2 and L^3 are shown in Fig. 3 (see Fig. S11 for full UV-visible spectra of the ligands).

The weak absorption band experimentally observed above 400 nm for the three ligands were computed at λ_{calc} = 398 nm (f = 0.03), λ_{calc} = 520 nm (f = 0.03) and λ_{calc} = 466 nm (f = 0.03) for L^1, L^2 and L^3, respectively. In all three cases, the acceptor fragment was a π orbital delocalized on the C(2), C(3), C(4) and C(5) carbon atoms and the donor fragment was a π orbital delocalized on the C(1), O(1), C(3), C(4) atoms of the cyclopentadienone ring. The nature of this transition was similar in all ligands and its position could be controlled through cyclopentadienone substitution. Indeed these results show that the transition is shifted to higher wavelengths *via* the introduction of electron-donating substituents on the C(3) and C(4) positions of the cyclopentadienone ring. Hughes *et al.* previously established that the lowering of this transition energy is due to the destabilization of π-donor orbitals located at the cyclopentadienone with a π*-acceptor orbital which does not vary in energy. For L^2, the intense band at 375 nm was computed at λ_{calc} = 342 nm (f = 0.38). The acceptor and donor fragments were π orbitals delocalized over the entire cyclopentadienone

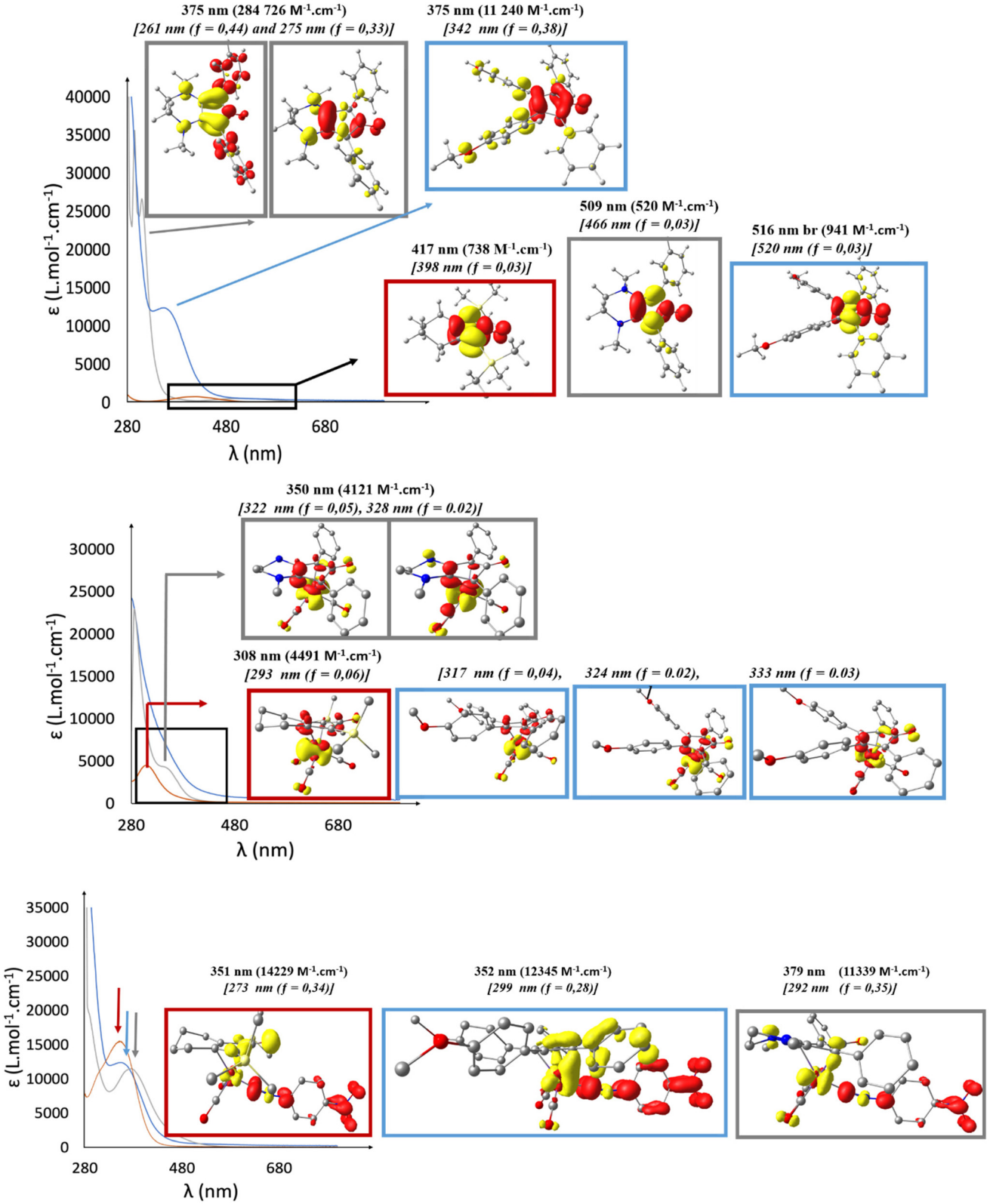

Fig. 3 UV-visible spectra of toluene solutions of ligands L^1 (brown line), L^2 (blue line), and L^3 (grey line) in 2.2×10^{-4} M in toluene (top figure), tris-carbonyl complexes **[FeL^1(CO)$_3$]** (brown line), **[FeL^2(CO)$_3$]** (blue line), and **[FeL^3(CO)$_3$]** (grey line) at 1×10^{-4} M in toluene (middle figure) and substituted complexes **[FeL^1(CO)$_2$(CN-Ph-NO$_2$)]** (brown line), **[FeL^2(CO)$_2$(CN-Ph-NO$_2$)]** (blue line), **[FeL^3(CO)$_2$(CN-Ph-NO$_2$)]** (grey line) at 2×10^{-4} M in toluene. T = 298 K. TD-DFT assignment of the electronic transitions of the ligands and complexes. Calculated wavelengths and oscillator strengths are noted in square brackets. Also shown are different electron densities where red corresponds to acceptor density and yellow to donor density.

Table 5 Electronic spectral data of the complexes and ligands[a]

Complex/Ligand	λ_{max}, nm (ε, M^{-1} cm^{-1})
L^1	417 (738)
[FeL^1(CO)$_3$]	308 (4491)
[FeL^1(CO)$_2$(CN-Ph-NO$_2$)]	351 (14 229), 308 sh (9466)
L^2	375 (11 240), 516 br (941)
[FeL^2(CO)$_3$]	279 br (24 887)
[FeL^2(CO)$_2$(CN-Ph-NO$_2$)]	352 (12 345), 281 (45 032)
L^3	314 (23 395), 509 (520)
[FeL^3(CO)$_3$]	284 (22 726), 350, sh, br (4121)
[FeL^3(CO)$_2$(CN-Ph-NO$_2$)]	284 (20 941), 379 (11 339)

[a] In toluene solution at 298 K. Abbreviations used: sh, shoulder; br, broad.

core and on the 2- and 5-phenyl rings, respectively. For L^3, the main transitions contributing to the strong absorption observed at 314 nm were computed at λ_{calc} = 261 nm (f = 0.44) and 275 nm (f = 0.33). In both cases, the donor fragment was a π orbital delocalized on the cyclopentadienone and fused rings while the π acceptor orbital was delocalized either on the C(2) and C(5) substituted phenyl rings or on the cyclopentadienone core. Altogether, these results show that irrespective of the substitution pattern, the ligands exhibit a weak absorption band involving π orbitals delocalized only on the cyclopentadienone core. In L^2 and L^3, the substitution of the C(3) and C(4) positions by either an electron-enriched fused ring or phenyl rings substituted in *para* positions by electron-donating substituents leads to the lowering of the energy of this transition and also to the appearance of strong absorption bands at lower wavelengths as compared to L^1.

Next, the effect of the cyclopentadienone ring substitution on the absorption properties of the tris-carbonyl complexes was investigated. **[FeL^1(CO)$_3$]** is characterized by a stronger absorption band at 308 nm (4491 M^{-1} cm^{-1}) as compared to the free L^1 ligand while the coordination of the $Fe^{(0)}(CO)_3$ moiety to the L^2 ligand leads to a partial loss of the transition of high intensity of the free ligand with **[FeL^2(CO)$_3$]** (blue line, Fig. 3), being characterized by a broad absorption band at a maximum located at 279 nm (24 887 M^{-1} cm^{-1}). In the case of **[FeL^3(CO)$_3$]**, the coordination of the $Fe^{(0)}(CO)_3$ moiety to the ligand induces the appearance of an absorption band at 350 nm (4121 M^{-1} cm^{-1}) while the strong absorption at a lower wavelength is 284 nm (22 726 M^{-1} cm^{-1}).

The exact nature of the orbitals involved in the UV-vis transitions of tris-carbonyl complexes was investigated using TD-DFT calculations. Difference density plots for the computed transitions responsible for the absorption of the complexes above 280 nm are shown in Fig. 3. For all complexes, the main electronic excitations contributing to the absorption above 280 nm are attributed to metal-to-ligand charge transfer (MLCT), with the donor orbital primarily localized on the iron center and the acceptor π* orbitals mostly delocalized over the cyclopentadienone core. The complexes **[FeL^2(CO)$_3$]** and **[FeL^3(CO)$_3$]** exhibit calculated transitions with higher oscillator strengths, which explains their stronger absorption around 280 nm compared to **[FeL^1(CO)$_3$]** (see Fig. S12 and S13). The occurrence of these transitions at higher wavelengths in **[FeL^2(CO)$_3$]** leads to the broadening of its MLCT absorption. It's interesting to see that the red shift of the MLCT by going from **[FeL^1(CO)$_3$]** to **[FeL^2(CO)$_3$]** and **[FeL^3(CO)$_3$]** is well reproduced by the calculations and attributed to the substitution of the cyclopentadienone core by the corresponding ligands.

Studies performed in our group had shown that with the L^1 based complex, the substitution of one CO by one isocyanide (CN-Ph-NO_2) led to the appearance of a new absorption band located at 351 nm (14 229 M^{-1} cm^{-1}) attributed to Fe 3d to CN π* orbital transitions with significant contribution from the phenyl-NO_2 part of the ligand (brown line, Fig. 3). More importantly, light-irradiation at a wavelength corresponding to the maximum absorption of this transition led to CO dissociation which allowed establishing a correlation between the catalytic activity of this complex under irradiation and its peculiar absorption properties. The same spectroscopic behavior is observed for **[FeL^2(CO)$_2$(CN-Ph-NO$_2$)]** (blue line, Fig. 3) and **[FeL^3(CO)$_2$(CN-Ph-NO$_2$)]** (grey line, Fig. 3) with the appearance of strong absorption bands located 352 nm (12 345 M^{-1} cm^{-1}) and 379 (11 339 M^{-1} cm^{-1}) as compared to **[FeL^2(CO)$_3$]** and **[FeL^2(CO)$_3$]** respectively. The TD-DFT calculations performed with the same methodology for the three complexes reveal that one main transition is responsible for the strong absorption experimentally observed. In all three complexes, the acceptor fragment is similar and corresponds to a CN π* orbital with a significant contribution from the phenyl-NO_2 part of the ligand. However, the nature of the donor fragment differs considerably. In **[FeL^1(CO)$_2$(CN-Ph-NO$_2$)]**, the donor corresponds to Fe 3d orbitals, with a contribution from the π orbital located on the carbonyl group of the cyclopentadienone. In contrast, in **[FeL^2(CO)$_2$(CN-Ph-NO$_2$)]** and **[FeL^3(CO)$_2$(CN-Ph-NO$_2$)]**, the donor is primarily composed of π orbitals delocalized over the entire cyclopentadienone, with a significant contribution from the 2- and 5-phenyl rings in **[FeL^2(CO)$_2$(CN-Ph-NO$_2$)]** or from the fused ring in the case of **[FeL^3(CO)$_2$(CN-Ph-NO$_2$)]**.

The absorption properties of the isocyanide complexes suggest that they possess the necessary characteristics to induce the photo-dissociation of one carbonyl ligand and the generation of the catalytically active species, as previously observed in the complex **[FeL^1(CO)$_2$(CN-Ph-NO$_2$)]**. In such a case, what can explain the poorer catalytic activity of the new complexes **[FeL^2(CO)$_2$(CN-Ph-NO$_2$)]** and **[FeL^3(CO)$_2$(CN-Ph-NO$_2$)]**? To answer this question, light-irradiation experiments were performed over time.

Firstly, we examined the behavior of **[FeL^2(CO)$_2$(CN-Ph-NO$_2$)]** under continuous irradiation in toluene at room temperature (Fig. 4a). A gradual and fast decrease of the absorption maximum at 359 nm and a concomitant increase of absorption bands at 284 nm and 525 nm were observed upon keeping the complex in solution under continuous irradiation at 368 nm over time (3 minutes total). Irradiation over longer times did not lead to further evolution of the UV-visible spectra and stopping the irradiation did not give back the initial spectrum indicating the fast and irreversible formation

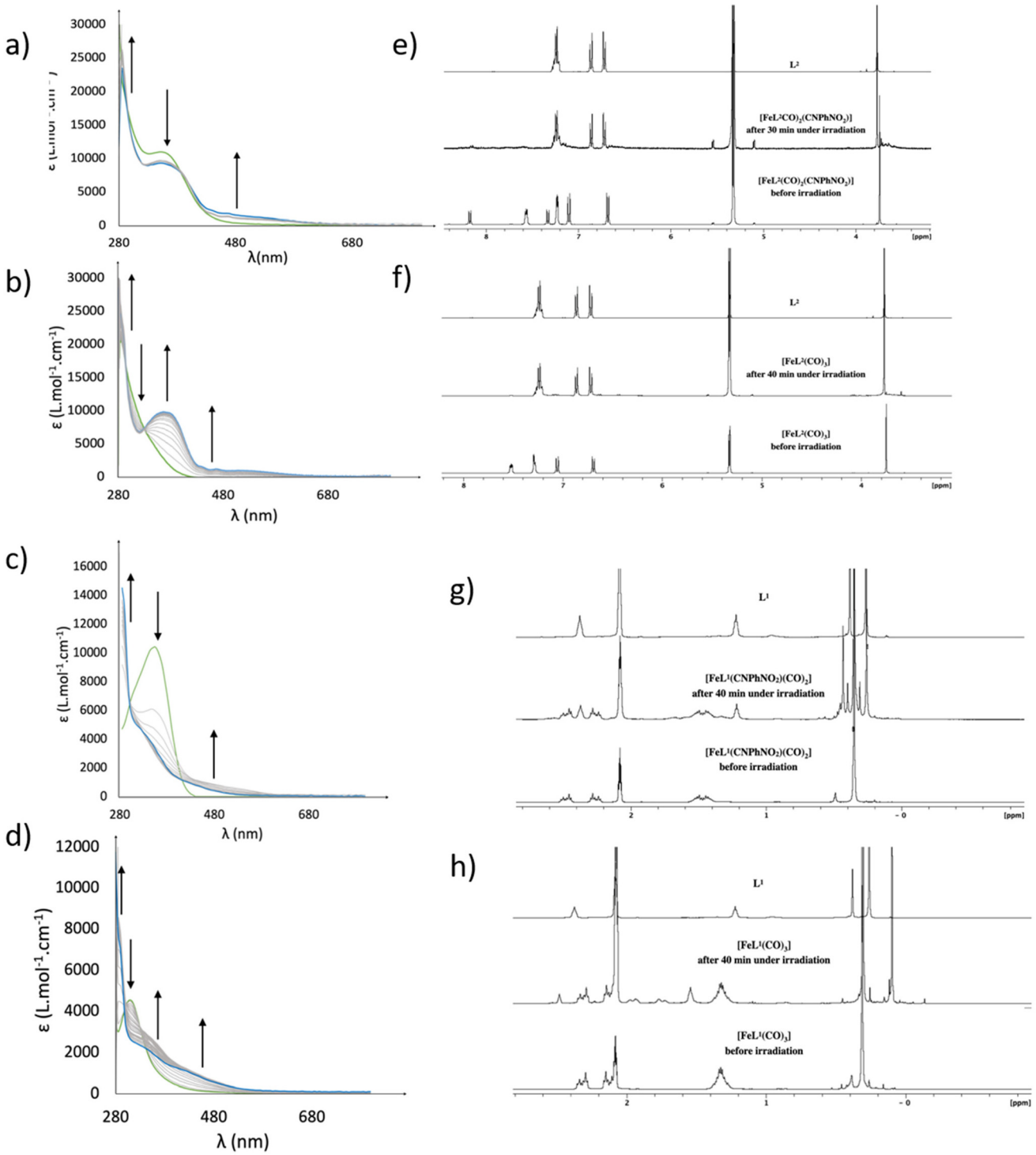

Fig. 4 Evolution of the UV-visible spectra of a solution of (a) **[FeL^2(CO)$_2$(CN-Ph-NO$_2$)]** (2.2 × 10^{-5} M), (b) **[FeL^2(CO)$_3$]** (2.2 × 10^{-5} M), (c) **[FeL^1(CO)$_2$(CN-Ph-NO$_2$)]** (7.3 × 10^{-5} M) and (d) **[FeL^1(CO)$_3$]** (7.3 × 10^{-5} M) in toluene at room temperature under an argon atmosphere and irradiation (368 nm ± 5 nm, 30 W). 45 scans; 1 scan each 4 seconds. Green and blue spectra correspond to the initial complex without irradiation and the final spectra after 45 scans, respectively. Time-dependent ^{1}H NMR studies over light irradiation in CD_2Cl_2 solvent (e) **[FeL^2(CO)$_2$(CN-Ph-NO$_2$)]**, (f) **[FeL^2(CO)$_3$]** and in $CDCl_3$ solvent (g) **[FeL^1(CO)$_2$(CN-Ph-NO$_2$)]** and (h) **[FeL^1(CO)$_3$]**.

of a stable species whose absorption properties look like those of the free ligand L^2. Surprised by these results, we examined the irradiation-dependent absorption changes of **[FeL^2(CO)$_3$]** under the same conditions (Fig. 4b). Here again we observed a fast, gradual and irreversible evolution of the initial spectrum with the appearance of two absorption bands at 370 nm and

509 nm and a decrease of the absorption at 326 nm (2.3 minutes total of continuous irradiation). The resemblance to the absorption spectrum of the free ligand and the presence of isobestic points suggest that irradiation leads to demetallation of the complex. Time-dependent ^{1}H NMR studies were performed under the same irradiation conditions and confirmed the fast and irreversible demetallation of both complexes **[FeL^2(CO)$_3$]** and **[FeL^2(CO)$_2$(CN-Ph-NO$_2$)]** under irradiation (Fig. 4e and f). Similar studies were conducted on **[FeL^3(CO)$_3$]** and **[FeL^3(CO)$_2$(CN-Ph-NO$_2$)]**, and the results exhibited a similar trend (demetallation) (Fig. S9).

However, **[FeL^1(CO)$_2$(CN-Ph-NO$_2$)]** and **[FeL^1(CO)$_3$]** exhibit different behaviors under photoactivation (Fig. 4c and d). On the one hand, after 40 minutes under continuous irradiation of the complex **[FeL^1(CO)$_2$(CN-Ph-NO$_2$)]**, the signal of the corresponding ligand was observed but the initial complex remained in a large proportion. On the other hand, **[FeL^1(CO)$_3$]** was the major species after 40 minutes of irradiation and a new and unidentified species had been formed. This new species clearly differed from the free L^1 ligand. Several attempts to isolate it failed and it was putatively attributed to the formation of an iron dimer complex. Indeed, DFT calculations show that in the absence of a substrate, the formation of a dimer species from a monomer after CO loss is favored. For the **[FeL^1(CO)$_2$(CN-Ph-NO$_2$)]** case, dimer formation is favored as $\Delta G = -8$ kcal mol^{-1} while ΔG of dimerization is -5 kcal mol^{-1} for **[FeL^1(CO)$_3$]** (Fig. 5b). Previous works have proposed such a dimer as the resting state.[4g] Alternatively, a dimer where the cyclopentadienone carbonyl oxygens coordinate to the empty sites on Fe was considered (Fig. 5c). That type of compound has been isolated for the Ru analogues of these compounds.[16] DFT calculations show that the formation of such a dimer species is even more likely. For both complexes ([**FeL^1(CO)$_2$(CN-Ph-NO$_2$)**] and **[FeL^1(CO)$_3$]**), such dimer formation is favored as $\Delta G = -12$ kcal mol^{-1}.

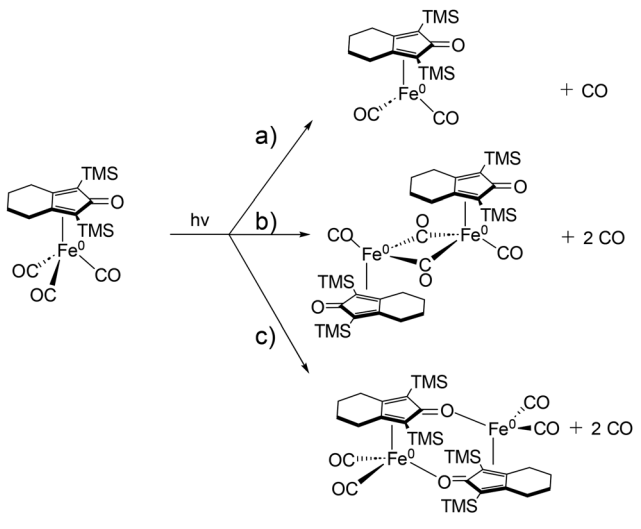

Fig. 5 Putative species formed under irradiation of **[FeL^1(CO)$_3$]**.

Altogether, these results show that complexes based on the L^1 type ligand are much more resistant to demetallation under irradiation at 365 nm explaining their excellent catalytic activity under photo-activation as compared to complexes based on L^2 and L^3 ligands. Bütikofer and Chen have shown that ligand exchange may occur in carbonyl-bridged dimers, leading to either catalyst deactivation *via* reversion to a tris-carbonyl complex or, more critically, demetallation and irreversible catalyst deactivation.[17] Although demetallation *via* dimer formation could not be experimentally confirmed for L^2 and L^3 based complexes—due to the inability to trap intermediates and the complete inhibition of the reaction upon addition of a chemical trap (see the SI)—this mechanism remains a plausible hypothesis. If the photo-irradiation of the complexes leads to their demetallation, how can the observed catalytic activity (low but still persistent) be explained? We hypothesize that the presence of an exogenous ligand (such as a substrate) could alter this process and prevent the demetallation to different extents depending on the cyclopentadienone ligand. To investigate this hypothesis the photo-irradiation of the complexes was performed in the presence of a stabilizing PPh$_3$ ligand (σ donor, π acceptor).

Behavior and species formed under irradiation of the complexes in the presence of an exogenous ligand

A previous experiment, carried out under 368 nm irradiation, with **[FeL^1(CO)$_2$(CN-Ph-NO$_2$)]** in the presence of a stabilizing exogenous PPh$_3$ ligand, led to the formation of a mixture of unreacted **[FeL^1(CO)$_2$(CN-Ph-NO$_2$)]** (27%) and a new species **[FeL^1(CO)(PPh$_3$)(CN-Ph-NO$_2$)]** in 60% isolated yield which could be characterized by XRD (Fig. 6) and NMR.[8] The analysis of the structure revealed that one terminal CO had been substituted by one PPh$_3$ ligand. Calculations further confirmed that the substitution of one CO ligand by PPh$_3$ was ∼4 kcal mol^{-1} more favorable (ΔG) than substitution of the isonitrile ligand. These results thus strongly suggest the decoordination of one terminal CO to occur under irradiation and the generation of an activated species whose structure differs from the classical **[FeL(CO)$_2$]**.

Similar experiments were conducted in the case of **[FeL^2(CO)$_2$(CN-Ph-NO$_2$)]**. Examination of the time-dependent UV-visible spectra of an irradiated solution of **[FeL^2(CO)$_2$(CN-Ph-NO$_2$)]** revealed a different trend in the presence of 2 equivalents of PPh$_3$ with a decrease of the absorption band at 352 nm and an increase of the band at 317 nm

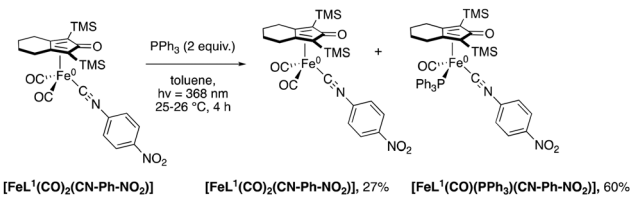

Fig. 6 Irradiation of **[FeL^1(CO)$_2$(CN-Ph-NO$_2$)]** in the presence of the exogenous PPh$_3$ ligand.

without a clear isosbestic point (Fig. 7). The absence of a clear isobestic point suggests the formation of more than one type of new species, most likely substituted complexes with PPh_3. The spectroscopic fingerprint of the free ligand L^2 was not observed in this case demonstrating that the irradiation does not lead to its photodissociation or only in small proportions.

In order to identify the type of species formed we performed ^1H and ^{31}P NMR experiments under the same irradiation conditions. The analysis of the ^1H NMR data (Fig. S5a) showed the complete disappearance of the signals of the initial **[FeL^2(CO)$_2$(CN-Ph-NO$_2$)]** complex and the appearance of a new set of signals after irradiation differing from those of the free ligand L^2 while ^{31}P NMR data (Fig. S5b) revealed the consumption of free PPh_3 ligand at −5.6 ppm and the appearance of two new signals at 59.0 ppm (major species) and 61.5 ppm (minor species). Purification of this mixture by chromatography column under air and the analysis of the isolated species led to the doubtless attribution of the ^{31}P NMR signal at 59.0 ppm to the formation of the substituted complex **[FeL^2(CO)(PPh$_3$)(CN-Ph-NO$_2$)]** (see SI page S9, an isolated yield of 64%) and a portion of the free cyclopentadienone ligand which was not identified in the case of the irradiation of **[FeL^1(CO)(PPh$_3$)(CN-Ph-NO$_2$)]**. These studies clearly show that the presence of an exogenous strongly stabilizing PPh_3 ligand mitigates the demetallation of the complex **[FeL^2(CO)$_2$(CN-Ph-NO$_2$)]**, albeit at the expense of the reactivity (see the SI for details). Under the multicatalytic reaction, the alcohol or the diketone would not stabilize the catalyst enough to prevent its decomposition over time.

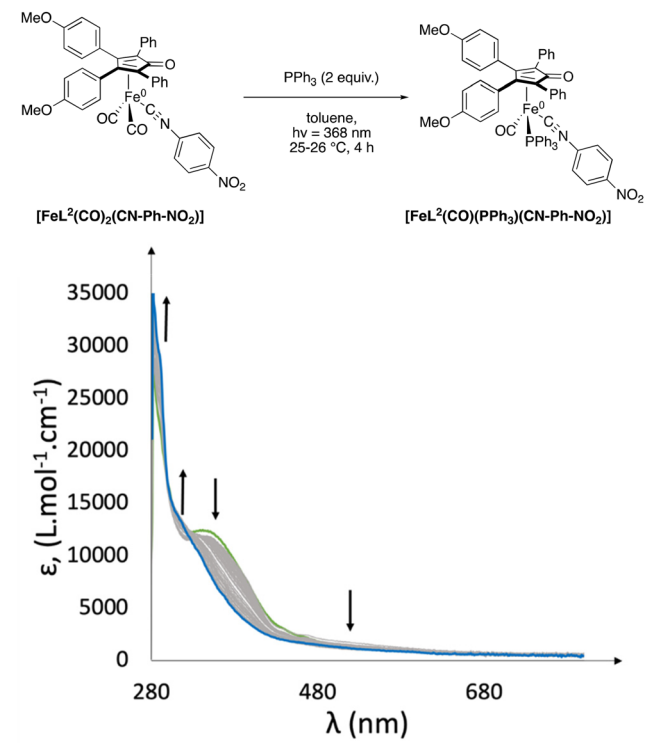

Fig. 7 Evolution of the UV-visible spectra of a solution of **[FeL^2(CO)$_2$(CN-Ph-NO$_2$)]** at 2.2 × 10^{-5} M in toluene in the presence of 2 equivalents of PPh_3 at room temperature under an argon atmosphere and irradiation (368 nm ± 5 nm, 30 W). 45 scans; 1 scan every 4 seconds. Green and blue spectra correspond to the initial complex without irradiation and the final spectrum after 45 scans, respectively.

Conclusions

In conclusion, a new family of 4-nitrophenyl isonitrile-substituted iron cyclopentadienone complexes was successfully prepared. Their design involved combining bis-carbonyl-isonitrile-iron, identified as the most promising moiety for efficient photocatalytic BH activity, with various electron-enriched cyclopentadienones, which have demonstrated superior catalytic efficiency for hydrogenation and/or dehydrogenation reactions under chemical activation. Surprisingly, the newly designed complexes exhibited significantly lower reactivity than the classical Knölker complex substituted with 4-nitrophenyl isonitrile.

Characterization of their physical properties, combined with DFT calculations, provided insights into their behavior under photo-irradiation and helped establish correlations with their reactivity. The extinction coefficients of the different complexes at the irradiation wavelengths vary significantly, as shown by both our experimental UV-vis spectra and computed oscillator strengths. This variation may imply different steady-state concentrations of the photoactivated species for each complex, and differences in the quantum yield—although not measured here—could further contribute to the reactivity. While we cannot at present determine the absolute concentrations of the active species under our reaction conditions, such variations could influence the observed catalytic performances. Nevertheless, our results demonstrate that, regardless of the initial concentration of the active species, the primary cause of catalyst deactivation is ligand-dependent demetallation. This mechanistic pathway remains the central finding of this study, with implications for the design of more robust photoactivated base-metal catalysts.

Indeed, prolonged photo-irradiation of the tris-carbonyl or isocyanide-substituted complexes bearing L^2 and L^3-type ligands clearly indicated complete demetallation. This phenomenon is mitigated by the presence of an exogenous ligand, which could explain the partial reactivity observed under catalytic conditions. In contrast, the resistance of complexes bearing the L^1-type ligand to photo-bleaching clearly accounts for their much higher activity compared to the others.

This underscores the importance of selecting isonitrile and cyclopentadienone ligands that are compatible with the chosen activation mode to achieve optimal reactivity. Indeed, while electron-enriched ligands provided better reactivity compared to iron complexes based on the classical L^1 ligand under chemical activation, they reduced the efficiency of the corresponding complexes under photoactivation by making them more prone to demetallation. Further design of catalysts by introducing various electron-enriched cyclopentadienone

ligands compatible with the photoactivation is currently underway in our laboratory. Given the significance of this class of catalysts and their activation *via* photochemical pathways, we hope that these studies will guide readers in designing catalysts tailored to their chosen activation method.

Author contributions

The manuscript was written through contributions of all authors. All authors have given approval to the final version of the manuscript.

Conflicts of interest

The authors declare no competing financial interests.

Data availability

The data supporting this article have been included as part of the SI: experimental protocols, detailed analysis, and additional experiments. See DOI: **https://doi.org/10.1039/d5dt01184a**.

CCDC 2419951 contains the supplementary crystallographic data for this paper.[18]

Acknowledgements

The Centre National de la Recherche Scientifique (CNRS), Université Grenoble-Alpes, the Commissariat à l'énergie Atomique, the Agence Nationale de la Recherche (ANR-23-CE07-0043) and the Labex ARCANE and CBH-EUR-GS (ANR-17-EURE-0003) are warmly acknowledged for financial support. All technical support staff from LCBM, DCM and ICMG are acknowledged for their help. Anestis Alexandridis is acknowledged for the UV reactor set-up.

References

1 (*a*) A. Quintard and J. Rodriguez, Iron Cyclopentadienone Complexes: Discovery, Properties, and Catalytic Reactivity, *Angew. Chem., Int. Ed.*, 2014, **53**, 4044–4055; (*b*) L. Pignataro and C. Gennari, Recent Catalytic Applications of (Cyclopentadienone) Iron Complexes, *Eur. J. Org. Chem.*, 2020, 3192–3205; (*c*) M. Akter and P. Anbarasan, (Cyclopentadienone) Iron Complexes: Synthesis, Mechanism and Applications in Organic Synthesis, *Chem. – Asian J.*, 2021, **16**, 1703–1724.

2 For initial discoveries in hydrogenation and hydrogen transfer, see: (*a*) C. P. Casey and H. Guan, An Efficient and Chemoselective Iron Catalyst for the Hydrogenation of Ketones, *J. Am. Chem. Soc.*, 2007, **129**, 5816–5817; (*b*) C. P. Casey and H. Guan, Cyclopentadienone Iron Alcohol Complexes: Synthesis, Reactivity, and Implications for the Mechanism of Iron-Catalyzed Hydrogenation of Aldehydes, *J. Am. Chem. Soc.*, 2009, **131**, 2499–2507.

3 For a selection of borrowing hydrogen reactions using such iron complexes, see: (*a*) A. Quintard, T. Constantieux and J. Rodriguez, An Iron/Amine-Catalyzed Cascade Process for the Enantioselective Functionalization of Allylic Alcohols, *Angew. Chem., Int. Ed.*, 2013, **52**, 12883–12887; (*b*) M. Roudier, T. Constantieux, A. Quintard and J. Rodriguez, Enantioselective Cascade Formal Reductive Insertion of Allylic Alcohols into the C(O)–C Bond of 1,3-Diketones: Ready Access to Synthetically Valuable 3-Alkylpentanol Units, *Org. Lett.*, 2014, **16**, 2802–2805; (*c*) T. Yan, B. L. Feringa and K. Barta, Iron catalysed direct alkylation of amines with alcohols, *Nat. Commun.*, 2014, **5**, 5602–5608; (*d*) S. Elangovan, J.-B. Sortais, M. Beller and C. Darcel, Iron-Catalyzed α-Alkylation of Ketones with Alcohols, *Angew. Chem., Int. Ed.*, 2015, **54**, 14483–14486; (*e*) H.-J. Pan, T. W. Nga and Y. Zhao, Iron-catalyzed amination of alcohols assisted by Lewis acid, *Chem. Commun.*, 2015, **51**, 11907–11910; (*f*) A. J. Rawlings, L. J. Diorazio and M. Wills, C–N Bond Formation between Alcohols and Amines Using an Iron Cyclopentadienone Catalyst, *Org. Lett.*, 2015, **17**, 1086–1089; (*g*) M. Roudier, T. Constantieux, A. Quintard and J. Rodriguez, Triple Iron/Copper/Iminium Activation for the Efficient Redox Neutral Catalytic Enantioselective Functionalization of Allylic Alcohols, *ACS Catal.*, 2016, **6**, 5236–5244; (*h*) C. Seck, M. D. Mbaye, S. Gaillard and J.-L. Renaud, Bifunctional Iron Complexes Catalyzed Alkylation of Indoles, *Adv. Synth. Catal.*, 2018, **360**, 4640–4645; (*i*) A. Lator, S. Gaillard, A. Poater and J.-L. Renaud, Well-Defined Phosphine-Free Iron-Catalyzed N-Ethylation and N-Methylation of Amines with Ethanol and Methanol, *Org. Lett.*, 2018, **20**, 5985–5990; (*j*) K. Polidano, B. D. W. Allen, J. M. J. Williams and L. C. Morrill, Iron-Catalyzed Methylation Using the Borrowing Hydrogen Approach, *ACS Catal.*, 2018, **8**, 6440–6445; (*k*) A. Quintard, M. Roudier and J. Rodriguez, Multicatalytic Enantioselective Borrowing Hydrogen δ-Lactonization Strategy from β-Keto Esters and Allylic Alcohols, *Synthesis*, 2018, **50**, 785–792; (*l*) D. E. Latham, K. Polidano, J. M. J. Williams and L. C. Morrill, One-Pot Conversion of Allylic Alcohols to α-Methyl Ketones via Iron-Catalyzed Isomerization–Methylation, *Org. Lett.*, 2019, **21**, 7914–7918; (*m*) L. Bettoni, S. Gaillard and J.-L. Renaud, Iron-Catalyzed β-Alkylation of Alcohols, *Org. Lett.*, 2019, **21**, 8404–8408; (*n*) L. Bettoni, S. Gaillard and J.-L. Renaud, Iron-Catalyzed α-Alkylation of Ketones with Secondary Alcohols: Access to β-Disubstituted Carbonyl Compounds, *Org. Lett.*, 2020, **22**, 2064–2069; (*o*) N. Shao, J. Rodriguez and A. Quintard, Catalysis Driven Six-Step Synthesis of Apratoxin A Key Polyketide Fragment, *Org. Lett.*, 2022, **24**, 6537–6542; (*p*) J. Wu, A. Tongdee, M. Cordier and C. Darcel, Selective Iron Catalyzed Synthesis of N-alkylated Indolines and Indoles, *Chem. – Eur. J.*, 2022, **28**, e202201809; (*q*) A. Alexandridis, T. Rancon, A. Halliday,

A. Kochem and A. Quintard, Iron- and Organo-Catalyzed Borrowing Hydrogen for the Stereoselective Construction of Tetrahydropyrans, *Org. Lett.*, 2024, **26**, 5788–5793.

4 For the initial studies on these complexes, see: (*a*) H.-J. Knölker, J. Heber and C. H. Mahler, Transition Metal-Diene Complexes in Organic Synthesis, Part 14.1 Regioselective Iron-Mediated [2 + 2 + 1] Cycloadditions of Alkynes and Carbon Monoxide: Synthesis of Substituted Cyclopentadienones, *Synlett*, 1992, 1002–1004; (*b*) A. J. Pearson, R. J. Shively Jr. and R. A. Dubbert, Iron Carbonyl Promoted Conversion of alpha,omega-Diynes to (Cyclopentadienone) iron Complexes, *Organometallics*, 1992, **11**, 4096–4104; (*c*) H.-J. Knölker and J. Heber, Transition Metal-Diene Complexes in Organic Synthesis, Part 18.1 Iron-Mediated [2 + 2 + 1] Cycloadditions of Diynes and Carbon Monoxide: Selective Demetalation Reactions, *Synlett*, 1993, 924–926. For later applications in catalysis: (*d*) S. A. Moyer and T. W. Funk, Air-stable iron catalyst for the Oppenauer-type oxidation of alcohols, *Tetrahedron Lett.*, 2010, **51**, 5430–5433; (*e*) T. C. Johnson, G. J. Clarkson and M. Wills, (Cyclopentadienone)iron Shvo Complexes: Synthesis and Applications to Hydrogen Transfer Reactions, *Organometallics*, 2011, **30**, 1859–1868; (*f*) D. S. Mérel, M. Elie, J.-F. Lohier, S. Gaillard and J.-L. Renaud, Bifunctional Iron Complexes: Efficient Catalysts for C=O and C=N Reduction in Water, *ChemCatChem*, 2013, **5**, 2939–2945; (*g*) S. Moulin, H. Dentel, A. Pagnoux-Ozherelyeva, S. Gaillard, A. Poater, L. Cavallo, J.-F. Lohier and J.-L. Renaud, Bifunctional (Cyclopentadienone)Iron–Tricarbonyl Complexes: Synthesis, Computational Studies and Application in Reductive Amination, *Chem. – Eur. J.*, 2013, **19**, 17881–17890; (*h*) T.-T. Thai, D. S. Mérel, A. Poater, S. Gaillard and J.-L. Renaud, Highly Active Phosphine-Free Bifunctional Iron Complex for Hydrogenation of Bicarbonate and Reductive Amination, *Chem. – Eur. J.*, 2015, **21**, 7066–7070; (*i*) P. Gajewski, M. Renom-Carrasco, S. V. Facchini, L. Pignataro, L. Lefort, J. G. de Vries, R. Ferraccioli, U. Piarulli and C. Gennari, Synthesis of (R)-BINOL-Derived (Cyclopentadienone)iron Complexes and Their Application in the Catalytic Asymmetric Hydrogenation of Ketones, *Eur. J. Org. Chem.*, 2015, 5526–5536; (*j*) R. Hodgkinson, A. Del Grosso, G. Clarkson and M. Wills, Iron cyclopentadienone complexes derived from C2-symmetric bis-propargylic alcohols; preparation and applications to catalysis, *Dalton Trans.*, 2016, **45**, 3992–4005; (*k*) S. Vailati Facchini, J.-M. Neudörfl, L. Pignataro, M. Cettolin, C. Gennari, A. Berkessel and U. Piarullia, Synthesis of [bis(hexamethylene)cyclopentadienone]iron tricarbonyl and its application to catalytic reductions of C=O, *ChemCatChem*, 2017, **9**, 1461–1468; (*l*) A. Del Grosso, A. E. Chamberlain, G. J. Clarkson and M. Wills, Synthesis and applications to catalysis of novel cyclopentadienone iron tricarbonyl complexes, *Dalton Trans.*, 2018, **47**, 1451–1470; (*m*) C. A. M. R. van Slagmaat, K. C. Chou, L. Morick, D. Hadavi, B. Blom and S. M. A. De Wildeman, *Catalysts*, 2019, **9**, 790–813; (*n*) G. M. Fusi, T. Gandini, S. Gazzola, T. Grell, V. Colombo, L. Pignataro and U. Piarulli, Design, Synthesis and Catalytic Activity of (Cyclopentadienone)iron Complexes Containing a Stereogenic Plane and a Stereogenic Axis, *Chem. – Eur. J.*, 2023, **29**, e202302533; (*o*) A. Bütikofer and P. Chen, Cyclopentadienone Iron Complex-Catalyzed Hydrogenation of Ketones: An Operando Spectrometric Study Using Pressurized Sample Infusion-Electrospray Ionization-Mass Spectrometry, *Organometallics*, 2022, **41**, 2349–2364; (*p*) L. Hackl, L. P. Ho, D. Bockhardt, T. Bannenberg and M. Tamm, Tetraaminocyclopentadienone Iron Complexes as Hydrogenation Catalysts, *Organometallics*, 2022, **41**, 836–851; (*q*) Q. Gaignard Gaillard, L. Bettoni, D. Paris, C. Lequertier, J.-F. Lohier, S. Gaillard and J.-L. Renaud, Synthesis of Triaminocyclopentadienyl Iron(II) Tricarbonyl Complexes and Application to the Synthesis of Aminophosphines, *Adv. Synth. Catal.*, 2023, **365**, 3704–3712; (*r*) S. Manna, J. Peters, A. Bermejo-López, F. Himo and J.-E. Bäckvall, Mechanistic Studies on Iron-Catalyzed Dehydrogenation of Amines Involving Cyclopentadienone Iron Complexes, Evidence for Stepwise Hydride and Proton Transfer, *ACS Catal.*, 2023, **13**, 8477–8484; (*s*) B. Goel, H. Neugebauer, A. I. VanderWeide, P. Sánchez, R. A. Lalancette, S. Grimme, A. Hansen and D. E. Prokopchuk, Essential Roles of Cp Ring Activation and Coordinated Solvent During Electrocatalytic H_2 Production with Fe(CpN_3) Complexes, *ACS Catal.*, 2023, **13**, 13650–13662.

5 For a selection, see: (*a*) A. Berkessel, S. Reichau, A. von der Höh, N. Leconte and J.-M. Neudörfl, Light-Induced Enantioselective Hydrogenation Using Chiral Derivatives of Casey's Iron-Cyclopentadienone Catalyst, *Organometallics*, 2011, **30**, 3880–3887; (*b*) T. N. Plank, J. L. Drake, D. K. Kim and T. W. Funk, Air-Stable, Nitrile-Ligated (Cyclopentadienone)iron Dicarbonyl Compounds as Transfer Reduction and Oxidation Catalysts, *Adv. Synth. Catal.*, 2012, **354**, 597–601; (*c*) S. Elangovan, S. Quintero-Duque, V. Dorcet, T. Roisnel, L. Norel, C. Darcel and J.-B. Sortais, Knölker-Type Iron Complexes Bearing an N-Heterocyclic Carbene Ligand: Synthesis, Characterization, and Catalytic Dehydration of Primary Amides, *Organometallics*, 2015, **34**, 4521–4528; (*d*) A. Bütikofer and P. Chen, Zwitterionic Halido Cyclopentadienone Iron Complexes and Their Catalytic Performance in Hydrogenation Reactions, *Inorg. Chem.*, 2023, **62**, 4188–4196.

6 See ref. 4 andB. K. Werley, X. Hou, E. P. Bertonazzi, A. Chianese and T. W. Funk, Substituent Effects and Mechanistic Insights on the Catalytic Activities of (Tetraarylcyclopentadienone)iron Carbonyl Compounds in Transfer Hydrogenations and Dehydrogenations, *Organometallics*, 2023, **42**, 3053–3065.

7 I. Yagoub, M. Clémancey, P.-A. Bayle, A. Quintard, G. Delattre, G. Blondin and A. Kochem, Mössbauer spectroscopic and computational investigation of an iron cyclo-

pentadienone complex, *Inorg. Chem.*, 2021, **60**, 11192–11199.

8 G. Quintil, L. Diebold, G. Fadel, J. Pécaut, C. Philouze, M. Clémancey, G. Blondin, R. Jornsson, A. Quintard and A. Kochem, CO to Isonitrile Substitution in Iron Cyclopentadienone Complexes: A Class of Active Iron Catalysts for Borrowing Hydrogen Strategies, *ACS Catal.*, 2024, **14**, 7795–7805.

9 For the preparation of tris-isonitrile complexes, see: A. Bütikofer and P. Chen, Cyclopentadienone triisocyanide iron complexes: general synthesis and crystal structures of tris(2,6-dimethylphenyl isocyanide)(η^4-tetraphenylcyclopentadienone) iron and tris(naphthalen-2-yl isocyanide)(η^4-tetraphenylcyclopentadienone)iron acetone hemisolvate, *Acta Crystallogr., Sect. E:Crystallogr. Commun.*, 2023, **79**, 626–632.

10 For examples of photo-induced, iron cyclopentadienone complex activation, see ref. 5, 8 and (*a*) H.-J. Knölker, H. Goesmann and R. Klauss, A Novel Method for the Demetalation of Tricarbonyliron–Diene Complexes by a Photolytically Induced Ligand Exchange Reaction with Acetonitrile, *Angew. Chem., Int. Ed.*, 1999, **38**, 702–705; (*b*) B. Emayavaramban, P. Chakraborty, P. Dahiya and B. Sundararaju, Iron-Catalyzed α-Methylation of Ketones Using Methanol as the C1 Source under Photoirradiation, *Org. Lett.*, 2022, **24**, 6219–6223; (*c*) M.-S. Abdallah, N. Joly, S. Gaillard, A. Poater and J.-L. Renaud, Blue-Light-Induced Iron-Catalyzed α-Alkylation of Ketones, *Org. Lett.*, 2022, **24**, 5584–5589; (*d*) M. Waheed, M. A. Alsharif, M. Issa Alahmdi, S. Mukhtar and H. Parveen, Visible Light Promoted Iron-Catalyzed One-Pot Synthesis of 2-Arylimino-2H-Chromenes from 2-Hydroxybenzyl Alcohols and β- Ketothioamides at Room Temperature, *Eur. J. Org. Chem.*, 2023, e202300136; (*e*) M. Waheed, M. A. Alsharif, M. I. Alahmdi, S. Mukhtar and H. Parveen, Visible Light Promoted Iron-Catalyzed One-Pot Synthesis of 2-Arylimino-2H-Chromenes from 2-Hydroxybenzyl Alcohols and β- Ketothioamides at Room Temperature, *Eur. J. Org. Chem.*, 2023, e202300136; (*f*) D. Song, R. Chen, W. Huang, P. Yang, L. Chen, J. Zhang, F. Ling and W. Zhong, Room-Temperature Synthesis of α-Alkylated Indolin-2-ones via a Photo Assisted Iron Catalyzed Borrowing Hydrogen Reaction, *Adv. Synth. Catal.*, 2024, **366**, 1893–1898.

11 A. Lator, S. Gaillard, A. Poater and J. Renaud, Iron–Catalyzed Chemoselective Reduction of α,β–Unsaturated Ketones, *Chem. – Eur. J.*, 2018, **24**(22), 5770–5774.

12 H.-J. Knölker, J. Heber and C. H. Mahler, Transition Metal-Diene Complexes in Organic Synthesis, Part 14. [1] Regioselective Iron-Mediated [2 + 2 + 1] Cycloadditions of Alkynes and Carbon Monoxide: Synthesis of Substituted Cyclopentadienones, *Synlett*, 1992, 1002–1004.

13 H.-J. Knölker and J. Heber, Transition Metal-Diene Complexes in Organic Synthesis, Part 18. [1] Iron-Mediated [2 + 2 + 1] Cycloadditions of Diynes and Carbon Monoxide: Selective Demetalation Reactions, *Synlett*, 1993, 924–926.

14 A. Cingolani, C. Cesari, S. Zacchini, V. Zanotti, M. C. Cassani and R. Mazzoni, Straightforward Synthesis of Iron Cyclopentadienone N-Heterocyclic Carbene Complexes, *Dalton Trans.*, 2015, **44**(44), 19063–19067.

15 R. G. Potter and T. S. Hughes, Predicting the UV–Vis Spectra of Tetraarylcyclopentadienones: Using DFT Molecular Orbital Energies to Model Electronic Transitions of Organic Materials, *J. Org. Chem.*, 2008, **73**(8), 2995–3004.

16 M. J. Mays, M. J. Morris, P. R. Raithby, Y. Shvo and D. Czarkie, X-Ray Structure, Reactivity and Catalytic Properties of a (Cyclopentadienone)Ruthenium Dimer, $[(C_4Ph_4CO)(CO)_2Ru]_2$, *Organometallics*, 1989, **8**(5), 1162–1167.

17 A. Bütikofer and P. Chen, *Organometallics*, 2022, **41**(16), 2349–2364.

18 CCDC 2419951: Experimental Crystal Structure Determination, 2025, DOI: **10.5517/ccdc.csd.cc2m74yz**.